An Explicit Multi-Model Compressible Flow Formulation Based on the Full Potential Equation and the Euler Equations on 3D Unstructured Meshes[*]

Xiao-Chuan Cai [†] Marius Paraschivoiu [‡] Marcus Sarkis [§]

1 Introduction

The development of a multi-model formulation to simulate three dimensional compressible flows on parallel computers is presented. The goal is to reduce the overall time and memory required to simulate the flow by using locally selected cheaper and more computational efficient physical models without sacrificing the global fidelity of the simulation. Our approach involves splitting the computational domain into different fluid flow regions and using the full potential model instead of the Euler or Navier-Stokes equations in regions where this approximation is valid. We show numerically that solving the full potential equation in regions of irrotational flow is not only more efficient but also improves the accuracy; avoiding any numerical generation of entropy. The main considerations addressed in this paper are the full potential and the Euler coupling and the discretization of the interface conditions between these domains. We use a fully unstructured finite volume discretization for both the full potential and the Euler equations, and the interface condition is derived by imposing the discrete conservation laws in the control volumes shared by both flow regions. 3D transonic flow simulations around a NACA0012 airfoil are investigated.

Numerical simulations of fluid flow have sufficiently matured to be considered accurate for engineering design and analysis. However, for large scale simulations, the response time remains too large for the software to be used as an interactive tool even on the lastest supercomputers. While parallel computing reduces computation time proportionally to additional computational resource,

[*] The work was supported in part by the NSF grants ASC-9457534, ECS-9527169, and ECS-9725504.

[†] Dept. of Comp. Sci., Univ. of Colorado, Boulder, CO 80309. cai@cs.colorado.edu

[‡] Dept. of Comp. Sci., Univ. of Colorado, Boulder, CO 80309. marius@cs.colorado.edu

[§] Math. Sci. Dept., Worcester Poly. Inst., Worcester, MA 01609. msarkis@wpi.edu

new algorithms should be constructed to perform faster on new and existing resources. In this paper we describe the initial steps for the development of a multi-model formulation to decrease the computation time of three dimensional compressible flow simulations on unstructured grids.

Compressible fluid flow simulations needed for aerodynamic applications can be modeled with different degree of sophistication. The simplest model is the full potential equation which assumes inviscid, irrotational and isentropic flows. This equation is a single second-order nonlinear differential equation that is inexpensive with respect to the execution time and the memory requirement. Validity of the full potential equation is, however, restricted. The isentropic assumption of the potential flow model leads to inaccurate physics for transonic flows with strong shocks. The next level of approximation is the Euler equations which describe the complete behavior of inviscid compressible flows. The Euler equations are a coupled system of five nonlinear differential equations of first order. Note that this set of equations involves five field variables. Finally, the Navier-Stokes equations include the viscous effects needed for accurate modeling of the boundary layer. However, these equations are not only more time consuming to solve but also require an associated mesh that is stretched and very fine in viscous regions. Nevertheless, for complex flows with separation of the boundary layer, the Navier-Stokes equations are mandatory to provide an accurate simulation. Furthermore, for high Reynolds number flows, turbulence appears and needs to be modeled.

When considering transonic flows over a wing, three regions can be identified: the boundary layer, the region around the shock, and the farfield. A multi–model formulation can be used to combine the strength of each model described above. Indeed, a multi-model formulation will take advantage of the quick computational time associated with solving the full potential equation while capturing all the important features of the flow such as boundary layers and shocks using the Navier-Stokes equations and/or the Euler equations, respectively. Furthermore, we can benefit from the extensive experience of numerical methods and software developed over the years to solve these equations separately.

Numerical techniques for the solution of the full potential equation and the Euler/Navier-Stokes equations were developed respectively in the 1970s and in the 1980s [2, 10, 13, 15, 18]. Indeed, compressible flow around entire aircrafts have been simulated. For example, the full potential equation has been solved for a 747-200 transport configuration with wing, body, struts, and nacelles [23]. For the Euler model, calculations over a complete aircraft have been performed as early as in 1986 [15]. On the other hand, accurate viscous simulations at high Reynolds number over such complex geometries require enormous computational resources. Approximate solutions, i.e., with less than adequate number of mesh points, have been performed. A Navier-Stokes prediction for the F–18 wing and fuselage is presented in [6]. A discussion of the drastic difference in computational cost related to the choice of models can be found in [14].

However only recently have there been interests to couple these solvers to reduce the computational cost, to reduce the memory requirement and to improve the accuracy of the solution. Certainly, boundary layer coupling or thin layer Navier-Stokes coupling have been widely used but such approaches do not quite include all the physics we intend to incorporate [22]. For some mathematical description of coupling heterogeneous models for compressible flows we refer the readers to [19]. For three dimensional flows, it is shown in [1, 20] that the computation cost can be reduced by a factor of two for a Navier-Stokes/full potential coupling. Their formulation is based on a structured grid discretization where the full potential equation is solved using a finite difference method and the Navier-Stokes equations are solved either with a finite difference or a finite volume discretization. The saving is justified by the fact that two third to one half of the cells are outside the Navier-Stokes region. In general, the cost of the full potential solver can be considered negligible compared to the Navier-Stokes solver. Note that each region is solved alternatively, similar to a subdomain iterative method.

Our formulation differs from [1, 20] by providing a general finite volume approach and therefore ensure that the mass will also remain conserved at the discrete level. This approach also has the advantage of being readily extended to a coupled *implicit* scheme. While in [1, 20] each region is solved separately, we are expecting to improve convergence by solving the coupled system simultaneously. In addition, an unstructured discretization of the computational domain provides more flexibility to mesh complex geometry and for adaptive control of the numerical error. Lastly, a parallel version is implemented to obtain the reasonable execution time.

In this paper we address the initial step of this research. We first investigate the coupling between the full potential equation and the Euler equations. In addition to the computational savings, solving the full potential equation in the vicinity of the stagnation point is more accurate by avoiding the numerical entropy generated by Euler solvers at low Mach numbers. Furthermore, the full potential solver is less sensitive to the quality of the elements. Both the Euler and the Navier-Stokes solvers calculate convective fluxes through edges. When the surface of the control volume is different from the perpendicular surface of the edges, a numerical error is created. This error does not appear in the full potential discretization because fluxes are constants in each element. As mentioned above, a finite volume formulation is adopted to adequately interface these different solvers. An explicit approach is first considered to validate the spatial discretization but also as a precursor to the implicit implementation [17].

For simplicity, we address steady flows. For unsteady flows, it is required to have the temporal derivative of the density which is difficult to include in our explicit scheme because this derivation involves potential values of the neighboring control volumes. However, in an implicit solver such discretization can be easily included. As already mentioned, to obtain the most accurate flow simulation, the full Navier-Stokes equations need to be included in our multi-model formulation.

A more urgent objective, however, is to address some algorithmic extensions. First, we intend to develop an implicit scheme which is essential for large scale simulations [17]. The convergence rates reported with implicit schemes are much faster, in particular when using methods such as the overlapping Schwarz preconditioned GMRES methods [3]. In our formulation, the Jacobian matrix used in the implicit approach will include the spatial discretization of two or more equations. It is expected that such system is not positive definite and thus it is not clear how it can be solved efficiently or which preconditioner should perform well. Second, we plan to develop a procedure to automatically position the interface between the different computational domains based on the existing field variables (i.e., dynamic zonal configuration). Third, we need to consider load balancing for parallel computations, in particular when dynamic zonal configuration procedures will be used. Recall that different partial differential equations are solved in different regions but each equation does not require the same number of operations. One palliative is to decompose each region into subregions equal to the number of processors. By using such an approach, we can allocated one subregion of each type to each processor. Finally, we expect that the outcome of this research will lead to a dramatic reduction in computational time and memory resources to allow faster simulation of compressible flows including turbulent viscous effect, in particular for external aerodynamics applications.

In this paper we focus on the description of the two-model formulation. Section 2 describes the explicit full potential solver and the Euler solver with more emphasis on the full potential solver. In Section 3, we briefly introduce the coupled solver and compare two types of interface conditions with overlap and without overlap. To demonstrate the feasibility of our approach we solve a transonic flow over a NACA0012 airfoil at zero angle of attack which is analyzed in Section 4. We conclude with remarks and extensions in Section 4.

2 Simulation of compressible flows

Our interest lies in the numerical simulation of three dimensional compressible invisid flows. We assume that there is no external force or heat transfer. As described above, these flows can be modeled with the Euler equations or with the full potential equation for the particular case when the irrotational and isentropic flows assumption is satisfied. For simplicity of presentation, all the descriptions given in the paper are based on the first order finite volume discretization, and the extension to the $2nd$ order discretization is easy. All the numerical results presented in Section 4 are for, however, the $2nd$ order discretization.

2.1 The governing equations

Let $\Omega \subset \Re^3$ be the computational flow domain and Γ its boundary. The conservative form of the Euler equations is given by

$$\frac{\partial U}{\partial t} + \nabla \cdot F(U) = 0. \tag{1}$$

Here U contains the conservative variables, i.e., $U = (\rho, \rho u, \rho v, \rho w, \rho E)^T$. The explicit definitions of $F()$ can be found on page 87 of [11]. When the flow is irrotational, there exists a potential variable Φ satisfying the full potential equation

$$\frac{\partial \rho(\Phi)}{\partial t} + \nabla \cdot G(\Phi) = 0, \tag{2}$$

where $G(\Phi) = \rho \nabla \Phi$ and

$$\nabla \Phi = (u, v, w)^T. \tag{3}$$

In the rest of the paper, we shall refer to U as the Euler variable, which is a vector, and Φ as the full potential variable, which is a scalar.

By appealing to the isentropic flow assumption we can write the density ρ as a nonlinear function of the potential, such as

$$\rho(\Phi) = \rho_\infty \left(1 + \frac{\gamma - 1}{2} M_\infty^2 \left(1 - \frac{||\nabla \Phi||_2^2}{q_\infty^2}\right)\right)^{1/(\gamma-1)}. \tag{4}$$

There are two types of boundaries that bound the computational domain for external flows past bodies or obstacles: the farfield boundary and the solid wall boundary. On the solid wall boundary, Γ_w, the normal velocity, $\mathbf{v}_n$, is zero, since no mass crosses the boundary. On the farfield, Γ_∞, we impose an uniform free-stream state defined by the following parameters: the density, ρ_∞, the velocity vector, $\mathbf{v}_\infty$, the pressure, p_∞, and the Mach number M_∞. These conditions are given by

$$\mathbf{v}_n = 0, \quad \text{on} \quad \Gamma_w \tag{5}$$

and

$$\rho_\infty = 1, \quad \mathbf{v}_\infty = \begin{pmatrix} \cos(\alpha) \times \cos(\theta) \\ \sin(\theta) \\ \sin(\alpha) \times \cos(\theta) \end{pmatrix}, \quad p_\infty = \frac{1}{\gamma M_\infty^2} \quad \text{on} \quad \Gamma_\infty, \tag{6}$$

where α and θ are the angles of the flow direction (the angle of attack and the yaw angle, respectively).

2.2 The Euler solver

To solve the Euler equations, we take advantage of an existing code based on an unstructured finite volume discretization of the convective fluxes [7, 8]. The computational flow domain is divided into tetrahedrons to provide maximum flexibility for tessellating complex geometries. Euler variables are located at the vertices of the elements. This code uses a second order flux discretization based on the MUSCL (Monotonic Upwind Scheme for Conservative Laws) scheme [16]. A classical forward Euler method for time integration with a local time step size is chosen. Recall that we are only interested in solving the steady state and a simple time integration scheme offers more flexibility to be coupled with the full potential solver. The local time step size $\Delta t^n_{\tau^c_i}$ is defined for each control volume τ^c_i (with characteristic size $\|h^c_i\|$) by

$$\Delta t^n_{\tau^c_i} = \|h^c_i\| \frac{\text{CFL}}{C^n_{\tau^c_i} + \|\mathbf{U}^n_{\tau^c_i}\|_2}, \tag{7}$$

where CFL is a preselected positive number, $C^n_{\tau^c_i}$ is the sound speed and $\mathbf{U}^n_{\tau^c_i}$ is the velocity vector at the nth time step.

The spatial discretization of the boundary condition, (5)-(6), is obtained using a non-reflecting version of the flux–splitting scheme [7].

2.3 The full potential solver

A new finite volume full potential solver is developed to adequately interface with the existing Euler solver. Therefore, the same control volume is used and only the flux calculations are different. We describe now the spatial discretization of the mass flux required in this scheme.

2.3.1 The spatial discretization

The integral form of the full potential equation for the discrete volume τ^c_i is simply

$$\int_{\tau^c_i} \nabla \cdot G(\Phi) dA = 0. \tag{8}$$

Note that the sum of all τ^c_i covers the whole domain Ω, i.e., $\bar{\Omega} = \bigcup \bar{\tau^c_i}$. By analogy to the discretization of the Euler equations, the discretization here is accomplished by dividing the domain into tetrahedron elements, $\tau^h_{i,j}$. The potential variable is stored at the vertices. This choice is illustrated in Fig. 1 for two space dimensions. By using this discretization, the space of the potential solution is taken to be piecewise linear continuous functions in each element determined from the vertices values, Φ_i.

For the control volume τ^c_i associated with the dual mesh, we can write the discrete form of (8) as

$$\int_{\tau^c_i} \nabla(\rho \nabla \Phi) dA = \int_{\partial \tau^c_i} \rho \nabla \Phi \cdot \mathbf{n} \, dS = \sum_{\tau^h_{i,j}} \rho_{i,j} (\nabla \Phi)_{i,j} \cdot \mathbf{S}^c_{i,j}, \tag{9}$$

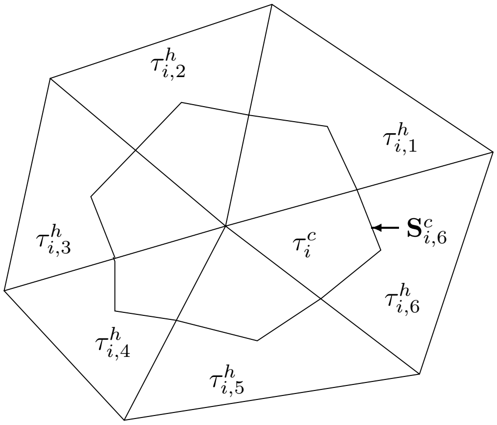

Figure 1: Two space dimensions representation of the control volume.

where $\tau^h_{i,j}$ is the "triangulation" associated with the control volume τ^c_i and $\mathbf{S}^c_{i,j} = \int_{\partial\tau^c_i \cap \tau^h_{ij}} \mathbf{n}\, dA$. Here $\mathbf{n}$ is the unit outward normal vector of the surface $\partial\tau^c_i \cap \tau^h_{ij}$. Note that $\rho_{i,j}$, the discrete density, is a function of $(\nabla\Phi)_{i,j}$ which is a constant for each element $\tau^h_{i,j}$.

2.3.2 An explicit approach

To solve (8) we add a time dependent term which vanishes at steady state. Hence, we rewrite (8) as

$$\frac{d}{dt}\int_{\tau^c_i} \Phi dA + \int_{\tau^c_i} \nabla \cdot G(\Phi) dA = 0. \tag{10}$$

The resulting semi-discrete form of (10) is

$$\|\tau^c_i\| \frac{d\Phi_i}{dt} + G_i(\Phi) = 0, \tag{11}$$

where G_i is the discretized mass flux associated with τ^c_i as in (9).

The system of ODE's associated with all control volumes is integrated in "time" using the forward Euler discretization. For a control volume τ^c_i, the equation is

$$\frac{\Phi^{n+1}_i - \Phi^n_i}{\Delta t^n_{\tau^c_i}} = -\frac{1}{\|\tau^c_i\|} G_i(\Phi^n). \tag{12}$$

The time step size $\Delta t^n_{\tau^c_i}$ is determined in the following way,

$$\Delta t^n_{\tau^c_i} = \min_{\tau^h_{i,j}} \left(C \|h^c_j\|^2 \right), \tag{13}$$

where $\|h_j^c\|$ is the characteristic length of element $\tau_{i,j}^h$ and C is a global constant. Because of the nonlinearity of this equation, it is difficult to determine C analytically. However, based on our numerical experiments, C equal to 0.4 is a good approximation.

2.3.3 The density upwinding scheme

For transonic flows, upwinding is required; therefore, the density is modified to add artificial compressibility. The upwinding is introduced prior to the flux calculation after which the same subsonic procedure is used. For simplicity, we describe our upwinding method for two space dimensions. Following [12, 23], we write

$$\tilde{\rho} = \rho - \mu \mathbf{v} \cdot \nabla_{-} \rho, \tag{14}$$

where $\mathbf{v}$ is the normalized element velocity and $\nabla_{-}\rho$ is an upwind difference. In two space dimensions there are two cases to consider. Either the mass flux enter on one side (Fig. 2 a) or the mass flux enter through two sides (Fig. 2 b). It follows that the density for each case becomes

$$\begin{aligned} \tilde{\rho_j} &= \rho_j + \mu \mathbf{v} \cdot \mathbf{n}_k (\rho_j - \rho_k) && (15) \\ \tilde{\rho_j} &= \rho_j + \mu \mathbf{v} \cdot \mathbf{n}_k (\rho_j - \rho_k) + \mu \mathbf{v} \cdot \mathbf{n}_\mathbf{l} (\rho_\mathbf{j} - \rho_\mathbf{l}). && (16) \end{aligned}$$

The switching function, μ, is defined for each element as

$$\mu = \nu_o \max\{0, 1 - M_c^2/M^2\}, \tag{17}$$

where M is the element Mach number, M_c is a pre-selected cutoff Mach number chosen to introduce dissipation in the transonic regime. The parameter ν_o is used to increase the amount of dissipation in the supersonic elements. These parameters M_c and ν_o are selected by hand; M_c is just smaller than 1 and ν_o is usually set between 1 and 3. Additional viscosity is added by taking the switching function in each element to be the maximum value of all its immediate neighbors. We refer the readers to [4, 9] for more details.

2.3.4 The boundary conditions

The full potential spatial discretization of the boundary condition is now described. On solid boundaries, Γ_w, we apply the surface flow tangency condition. We write,

$$\rho \frac{\partial \Phi}{\partial n} = 0, \tag{18}$$

for solid wall at rest. In our control volume approach, this boundary condition is identical to no flux across the solid boundary. It is, therefore, straightforward to implement; we just sum the flux across the boundary of the control volume which are in the interior of the computational domain.

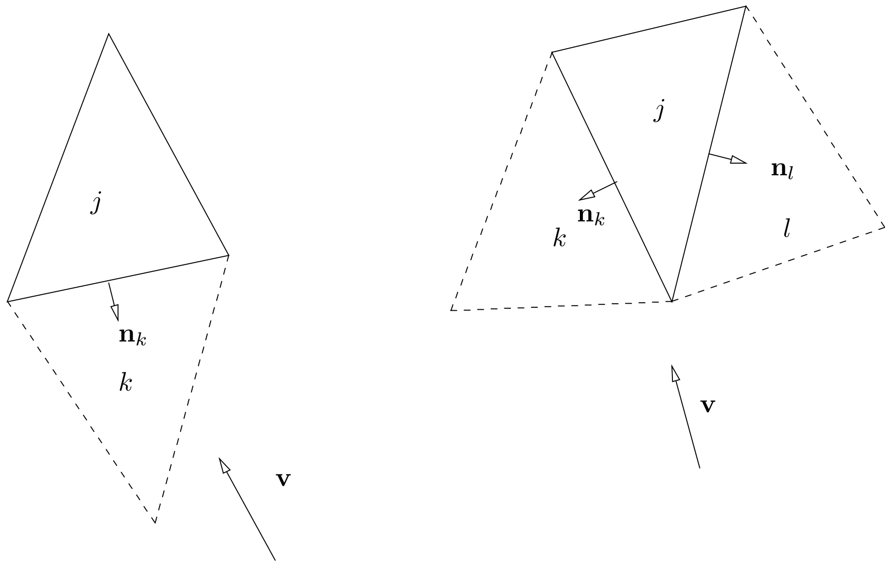

Figure 2: Upwind configurations.

For the farfield boundary, Γ_∞, we normalize the farfield flow speed, q_∞, to equal unity and we define the farfield potential as

$$\Phi_\infty = \int_\Omega q_\infty dx, \tag{19}$$

where x is the direction of the farfield flow. To enforce this Dirichlet boundary condition we impose the value of Φ_∞ in the control volumes which lie on the farfield boundary. It is also possible to replace the above condition with a more transparent condition such as imposing a mass flux associated with the free stream state. This condition is implemented on parts of Γ_∞ adjacent to the Euler domain. We recognize that these boundary conditions are simplistic and we recommend a boundary condition based on Riemann invariants [21] or on linearized Euler equations [5]. Furthermore, a farfield correction is required for lifting wings.

3 The coupled solver

The spatial computational domain, Ω, is split into two subdomains, Ω_E and Ω_Φ, wherein the Euler equations and the full potential equation are solved respectively. We denote by Γ_I the interface between Ω_E and Ω_Φ.

The formulation presented herein for the full potential is similar to the unsteady Euler formulation for finite volume. In fact, we can define W as the *simulation variable*, which represents either U or Φ. A general formulation can thus be constructed. In the future version of our software implementation, W will be a pointer and its true value and size are determined while the flow is being calculated. We assume that W is the solution of the equation

$$\frac{\partial W}{\partial t} + \nabla \cdot P(W) = 0, \tag{20}$$

where the flux function P is called the *model function* that equals to either F or G. The decision to choose a specific model will be made for each subdomain. However, the main part of this coupled solver is the treatment of the conservation law at the interface boundary.

3.1 The interface boundary conditions

There are several issues related to the interface boundary such as location, formulation and discretization. In this paper we mainly describe the discretization. We report on two different domain partitioning approaches: the overlapping and non-overlapping partitioning.

3.1.1 An overlapping partition

Consider the interface between the full potential domain and the Euler domain presented in Fig. 3. This interface is located between tetrahedra. Therefore the control volume associated with the nodes on this interface are shared between both the full potential domain and the Euler domain. These control volumes are considered as the overlapping region. Conservation laws for the Euler equations as well as the conservation laws for the full potential equation are forced on this control volume. First, we describe discretization of the conservation laws associated with the Euler equations, i.e., the conservation of mass, momentum and energy. The fluxes across the surface of the control volume that lies in the Euler domain (Ω_E) can be readily calculated. However, we require to convert the full potential variable to the Euler variable to calculate the fluxes across the surface that lies in the potential domain (Ω_Φ). To this end we use the potential to Euler variable transfer function (Appendix A) to calculate, at vertex, k and l for example, the momentum and the energy. These vertex values are obtained by the volume weighted averaging of the density and the velocity in the elements surrounding this vertex. Note that, the density and the velocity, $\nabla\Phi$, are constant in the elements laying in the full potential domain. Therefore, these Euler fluxes calculations depend on the Euler variable on one side and on the potential converted to mass, momentum and energy on the other side. We introduce an operator Q related to the transfer of the potential variable to the Euler variable defined as

$$U = Q(\Phi). \tag{21}$$

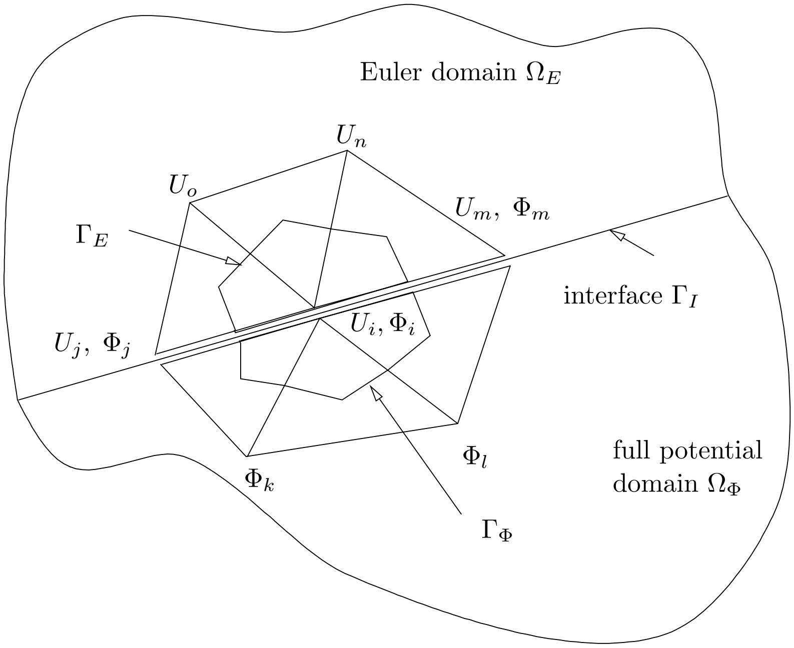

Figure 3: Overlapping interface of the Euler and full potential domains.

The interface condition for the Euler solver becomes

$$\int_{\Gamma_E} F(U) \cdot \mathbf{n}_E dS + \int_{\Gamma_\Phi} F(Q(\Phi)) \cdot \mathbf{n}_\Phi dS = 0, \tag{22}$$

where the subscript E and Φ refer to the Euler and the potential segments of the control volume, respectively.

Second, we present the conservation of mass for the same control volume required for the full potential solver. To be more precise the conservation of mass is written as

$$\int_{\Gamma_E} \rho V \cdot \mathbf{n}_E dS + \int_{\Gamma_\Phi} \rho \nabla\Phi \cdot \mathbf{n}_\Phi dS = 0, \tag{23}$$

where ρV is the first component of the Euler flux vector. These two integrals can be discretized into sums over the edges of the control volume, such as,

$$\sum_{\tau_{i,j}^h} \rho V \cdot \mathbf{S}_{i,j}^E + \sum_{\tau_{i,j}^h} \rho_{i,j} (\nabla\Phi)_{i,j} \cdot \mathbf{S}_{i,j}^\Phi = 0, \tag{24}$$

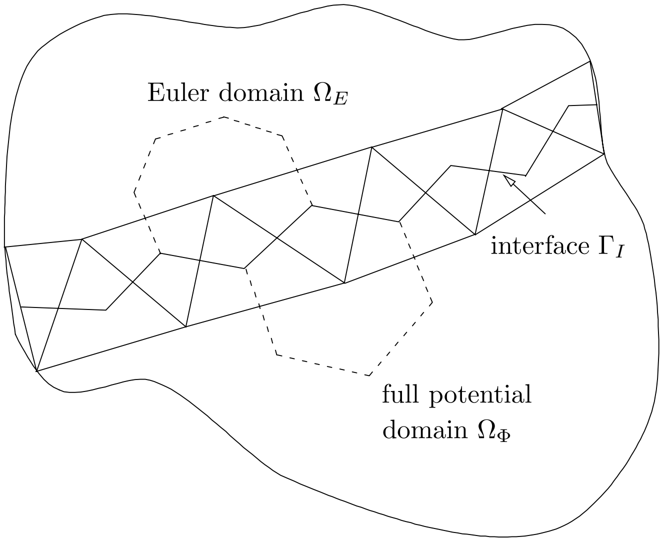

Figure 4: Non–overlapping interface of the Euler and full potential domains.

where $\mathbf{S}_{i,j}$ is the surface intergal of the outward normal vector along the j surface of the control volume τ_j^c associated with each element $\tau_{i,j}^h$. Note that in this approach we have over-determined the conservations laws. Indeed, the same control volume will satisfy the conservation of mass for both the Euler equations and for the full potential equation.

3.1.2 A non-overlapping partition

The non-overlapping domain permits a proper discretization of the equations without over-determining the conservation laws. In this approach, control volumes are flagged either for solving the full potential equation or for solving the Euler equations. The location of the interface, therefore, lies between the control volumes as in the two dimensional illustration in Fig. 4. The interface condition for the Euler solver is given by (22) where Γ_Φ is the portion of the control volume that lies on the interface Γ_I. The Euler fluxes through this control surface are calculated using the same procedure as in the interior of the Euler domain which is based on solving a Riemann problem defined on an edge using the two end–point nodal values. Because this edge crosses the interface, it contains the potential variable at one end and the Euler variable at the other. To use the same procedure, we convert the potential variable to the Euler variable. To convert Φ to U at one vertex, we use $\nabla\Phi$ in the tetrahedra surrounding that vertex. When the tetrahedron intersects the interface then an approximation of the velocity is used instead of $\nabla\Phi$.

The mass flux balance for the full potential control volume that lies on the interface is given by (23) where Γ_E is now the portion of the control volume that lies on the interface. The term ρV is the type first term in the Euler flux vector which is related to the conservation of mass. Clearly, this approach guarantees that the mass fluxes at the interface are conserved.

4 Computational results

4.1 Transonic flow passing a NACA0012 airfoil

In this section we present heterogeneous full potential and Euler solutions in three space dimensions. We test our scheme for a two dimensional flow over a NACA0012 airfoil at $M_\infty = 0.8$ in a three dimensional computational domain. However, only half of the geometry is required for this symmetric flow. The computational domain is such that Ω is a rectangle domain where an upper surface of a NACA0012 is located on the bottom face as presented in Fig. 5. The boundary conditions of this problem are as follows: on Γ_1, Γ_2, and Γ_3 we impose farfield conditions; on Γ_4, Γ_6, Γ_7, and Γ_8 we impose the non-penetration condition for symmetry and on Γ_5 we impose the solid wall condition. Note that, a non-penetration condition or a solid condition are identical. For the farfield boundary Γ_1, Γ_2, and Γ_3, the discretization of this condition differs for the full potential solver between Γ_2 where we impose Φ_∞ as a Dirichlet condition and Γ_1 and Γ_3 where we only specify a flux at the boundary. Concerning the switching function μ, the cutoff Mach number is set to $M_\infty^2 = 0.95$ and the viscous parameter is set to $\nu_o = 1.5$.

We present in Fig. 6 the mesh associated with the computational domain and the domain partitioning of this mesh into the Euler domain (bottom) and the full potential domain (top). The gap between the domains is artificially added for visual purpose. In our current implementation, the interface is hand-picked, and with such a partition the shock is contained completely in the Euler domain. Note that this mesh is also partitioned into eight subdomains for parallel processing. Each of the subdomains have more or less the same number of mesh points even thought ultimately the node distribution per processor should take into account the type of solver used. We show the Mach number contours for the overlapping and the non-overlapping partitions in Fig. 7 and Fig. 8, respectively. Note the smooth transition of the iso–contours between the Euler and full potential domains. The interface of the Euler and the full potential domains lies at the intersection of different processors. This interface is presented in Fig. 6. The flow domain is discretized into 16,200 control volumes and the solution was obtained after 80,000 explicit iterations.

We also report on the pressure coefficient distribution over the airfoil, Fig. 9. The solid line represents the Euler solution, the dash lines represent the full po-

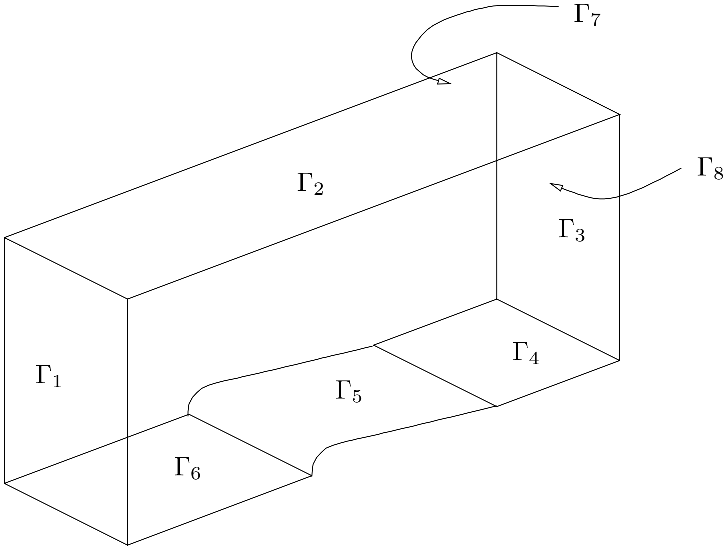

Figure 5: Computational domain for the NACA0012 geometry.

tential solution and the stars represent the coupled solution. Based on our numerical experience, we report that the full potential solution is very sensitive to the farfield boundary location. Clearly, the farfield boundary in our computational domain is still very close to the airfoil. On the other hand, the Euler solution is far less sensitive to the farfield boundary location. This hidden cost of the full potential should be accounted for when evaluating the cost reduction. The shock location in the full potential solution is therefore sensitive to the boundary location. However, in all the runs we have performed, we note that the coupled solution obtains a shock which is located upwind of the potential shock. The shock location also depends on the location of the interface between the two domains. In this case, we report that the shock in the coupled solution is at the same location as the Euler shock on the surface of the airfoil but differs slightly in the interior.

4.2 Remarks

Before concluding, we want to report on our numerical experience of the full potential and the Euler models coupling.

First, we observe that solutions are similar for the overlapping or the non-overlapping partitioning. The solution is smooth across the interface and the convergence rate is not significantly affected by the choice of overlapping or

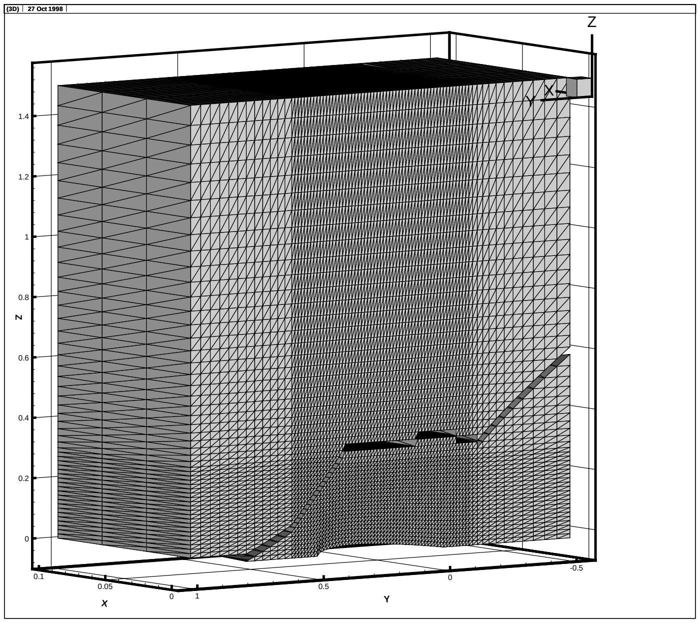

Figure 6: Computational mesh and domain decomposition for the NACA0012 airfoil.

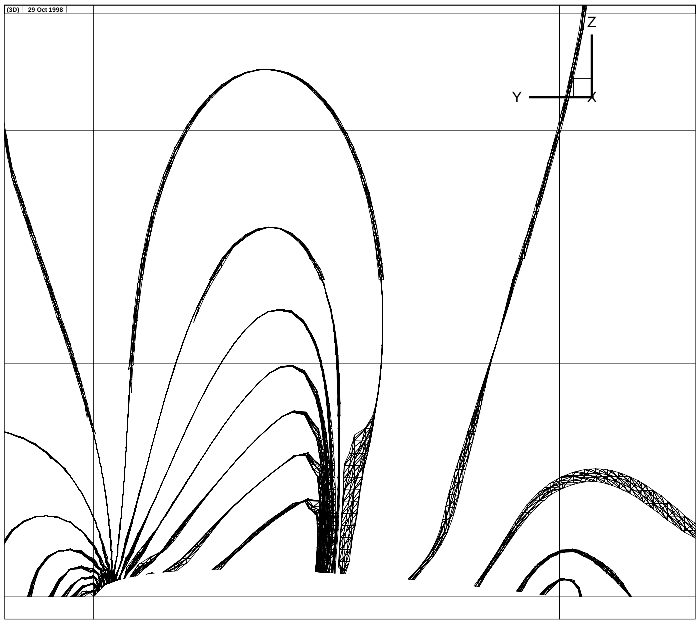

Figure 7: Mach number contours for the NACA0012 airfoil at $M_\infty = 0.8$ for overlapping domains.

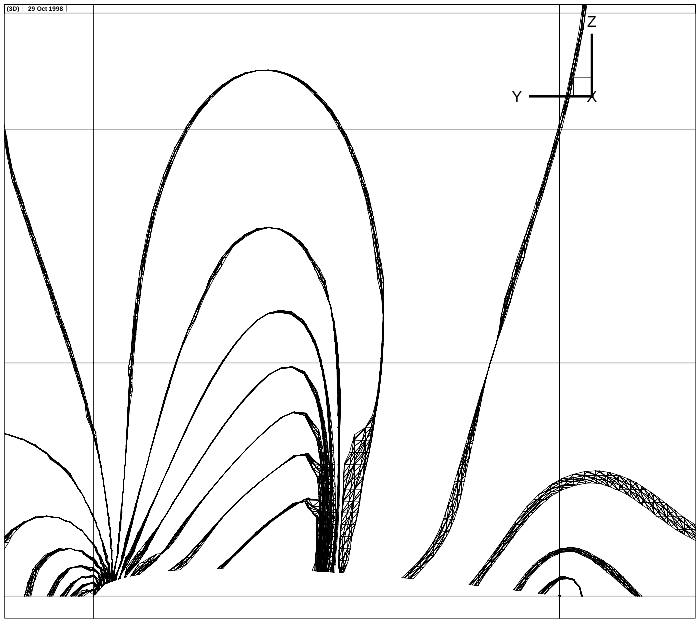

Figure 8: Mach number contours for the NACA0012 airfoil at $M_\infty = 0.8$ for non-overlapping domains.

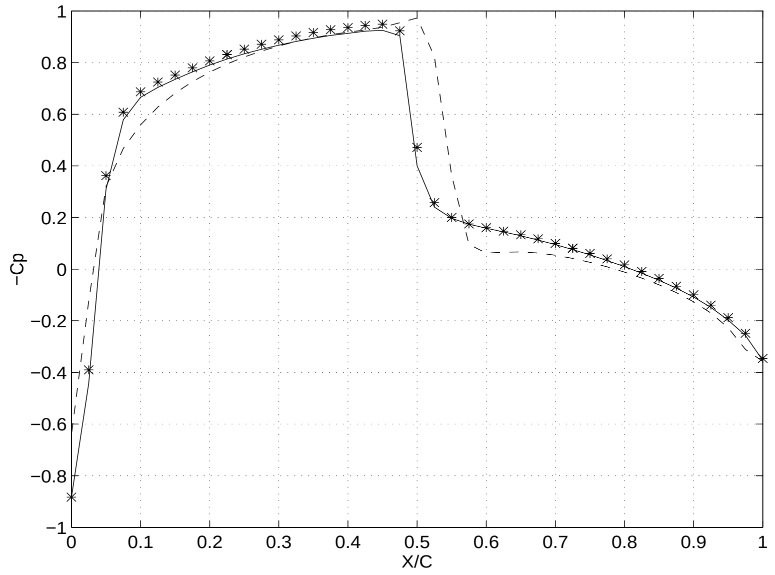

Figure 9: Pressure coefficient distribution on a NACA0012 airfoil at $M_\infty = 0.8$. — Euler solution; $--$ full potential solution; $*$ mixed solution.

non-overlapping approaches. The main difference is the added computational cost of calculating the Euler fluxes for the overlapping control volume and the storage associated with the existence of the overlapping control volume which has both the Euler variable and the potential variable. On the other hand the overlapping partitioning is required in implicit solutions using an overlapping Schwarz algorithm.

Second, for simplicity of presentation, the discretization presented herein has focused on the first order scheme for the Euler equations and for the interface discretization. For higher order schemes, we convert from potential to the Euler variable not only the vertex values of the control volume located on the interface but also the vertices of the neighbors such that the evaluation of the gradient of the solution at each vertex can be calculated. Indeed, the results presented in Section 4 are obtained using a second order scheme. A similar approach will be required when attempting the coupling with the Navier-Stokes equations.

Lastly, physical solutions for the full potential flow over a wing are obtained by imposing the Kutta condition; that the flow leaves the trailing edge smoothly. For a full potential solver such a condition is enforced by adding a jump in the potential equal to the circulation. Note that for non-lifting airfoils, as in our model problem, we do not need to enforce the Kutta condition. However, it is fortunate that the Euler solution of such flows intrinsically respects this condition. For future considerations such as lifting wings we will define the Euler domain to cover the wing and the wake region. With this partition we avoid any special treatment in the full potential domain because the full potential region does not cross the trailing edge vortex sheet.

5 Conclusions

In this paper we have showed the feasibility of coupling the Euler equations and the full potential equation in the simulations of three dimensional steady compressible flows. An explicit formulation was presented based on a forward Euler time integration scheme and a fully unstructured finite volume scheme for the spatial variables. Numerical results obtained on a distributed memory parallel computer were reported for a transonic flow passing a NACA0012 wing. We have also laid down the background to fully extend this formulation for multiple flow models and for different numerical approaches. We have not investigated the reduction in computation time because the fastest solvers are based on implicit approaches. The next step is to expand this formulation to the implicit approach and address the evaluation of computation time reduction as well as other parallel implementation issues.

6 Acknowledgments

We thank D. Keyes and D. P. Young for many stimulating discussions.

References

[1] M. E. Berkman, L. N. Sankar, C. R. Berezin, and M. S. Torok. Navier–Stokes/full potential/free–wake method for rotor flows. *J. of Aircraft*, 34:635–640, 1997.

[2] M. Bristeau, R. Glowinski, J. Periaux, P. Perrier, O. Pironneau, and C. Poirier. On the numerical solution of nonlinear problems in fluid dynamics by least squares and finite element methods (ii), application to transonic flow simulations. *Comput. Methods. Appl. Mech. Engrg.*, 51:363–394, 1985.

[3] X.-C. Cai, C. Farhat, and M. Sarkis. A minimum overlap restricted additive Schwarz preconditioner and applications in 3D flow simulations. In C. Farhat J. Mandel and X.-C. Cai, editors, *The Tenth International Conference on Domain Decomposition Methods for Partial Differential Equations.* AMS, 1998.

[4] X.-C. Cai, W. D. Gropp, D. E. Keyes, R. G. Melvin, and D. P. Young. Parallel Newton–Krylov–Schwarz algorithms for the transonic full potential equation. *SIAM J. Sci. Comput.*, 19:246–265, 1998.

[5] C. Coclici and W. L. Wendland. Domain decomposition methods and farfield boundary conditions for 2D compressible viscous flows. In *Proc. of ECCOMAS 98*, 1998.

[6] R. Cummings, Y. Rizk, L. Schiff, and N. Chaderjian. Navier–Stokes predictions for the F–18 wing and fuselage at large incidence. *J. of Aircraft*, 29:565–574, 1992.

[7] C. Farhat and S. Lanteri. Simulation of compressible viscous flows on a variety of MPPs: Computational algorithms for unstructured dynamic meshes and performance results. *Comput. Methods Appl. Mech. Engrg*, 119:35–60, 1994.

[8] C. Farhat, M. Lesoinne, P. S. Chen, and S. Lantéri. Parallel heterogeneous algorithms for the solution of the three–dimensional transient coupled aeroelastic problems. *AIAA Paper 95-1290*, 1995.

[9] W. G. Habashi and M. M. Hafez. Finite element solutions of transonic flow problems. *AIAA J.*, 20:1368–1375, 1982.

[10] M. Hafez, J. South, and E. Murman. Artificial compressibility method for numerical solution of the transonic full potential equation. *AIAA J.*, 17:838–844, 1979.

[11] C. Hirsch. *Numerical Computation of Internal and External Flows.* John Wiley and Sons, New York, 1990.

[12] T. L. Holst and W. F. Ballhaus. Fast, conservative schemes for the full potential equation applied to transonic flows. *AIAA J.*, 17:145–152, 1979.

[13] T. L. Holst, J. W. Slooff, H. Yoshihara, and W. F. Ballhaus. Applied computational transonic aerodynamics. Technical Report AG-266, AGARD, 1982.

[14] A. Jameson. Essential elements of computational algorithms for aerodynamics. Technical Report 97-68, ICASE, 1997.

[15] A. Jameson, T. Baker, and N. Weatherill. Calculation of inviscid transonic flow over a complete aircraft. *AIAA Paper 86-0103*, 1986.

[16] B. Van Leer. Towards the ultimate conservative difference scheme. V. A second order sequel to Godunov's method. *J. Comput. Phys.*, 32:361–370, 1979.

[17] M. Paraschivoiu, X.-C. Cai, M. Sarkis, D. P. Young, and D. Keyes. An implicit multi–model compressible flow formulation based on the full potential equation and the Euler equations. *AIAA Paper 99-0784*, 1999. To appear.

[18] R. B. Pelz and A. Jameson. Transonic flow calculations using triangular finite elements. *AIAA Paper 83–1922*, 1983.

[19] A. Quarteroni and A. Valli. *Domain Decomposition Methods for Partial Differential Equations.* Oxford University Press, Oxford, 1999.

[20] L. N. Sankar, B. K. Bharadvaj, and F. Tsung. Three-dimensional Navier–Stokes/full potential coupled analysis for transonic viscous flow. *AIAA J.*, 31:1857–1862, 1993.

[21] V. Shankar, H. Ide, J. Gorski, and S. Osher. A fast, time–accurate, unsteady full potential scheme. *AIAA J.*, 25:230–238, 1987.

[22] D. P. Young, R. G. Melvin, M. B. Bieterman, F. T. Johnson, and S. S. Samant. Global convergence of inexact Newton methods for transonic flow. *Int. J. Numer. Methods. Fluids*, 11:1075–1095, 1990.

[23] D. P. Young, R. G. Mervin, M. B. Bieterman, F. T. Johnson, S. S. Samant, and J. E. Bussoletti. A locally refined rectangular grid finite element methods: Application to computational fluid dynamics and computational physics. *J. Comput. Phys.*, 92:1–66, 1991.

A Transfer operators

To carry out our multi–model formulation, we do not require the transfer operator from Euler to potential $R : U \longrightarrow \Phi$. Only the mass flux, given by $G(R(U))$, is required to update the potential in each control volume. We define the full potential to Euler transfer operator as

$$Q : \Phi \longrightarrow U. \tag{25}$$

Recall that U has five components. To obtain its first component, we appeal to

$$\rho(\Phi) = \rho_\infty \left(1 + \frac{\gamma - 1}{2} M_\infty^2 \left(1 - \frac{||\nabla\Phi||_2^2}{q_\infty^2}\right)\right)^{1/(\gamma-1)}. \tag{26}$$

The next three components can be computed with relation (3). The last component ρE

$$\rho E = \rho \left(e + \frac{u^2 + v^2 + w^2}{2}\right) = \frac{p}{\gamma - 1} + \rho \frac{u^2 + v^2 + w^2}{2},$$

where the pressure

$$p = p_\infty \left(\frac{\rho}{\rho_\infty}\right)^\gamma.$$